IEEE Access
Multidisciplinary : Rapid Review : Open Access Journal

Received September 8, 2019, accepted October 2, 2019, date of publication October 7, 2019, date of current version October 18, 2019.

Digital Object Identifier 10.1109/ACCESS.2019.2946085

Optimization for a Locally Resonant Phononic Crystal of Square Spiral With Circle Inside

HANG XIANG[1], XINGFU MA[2], AND JIAWEI XIANG[2], (Member, IEEE)
[1]Department of Applied Physics, Tunghai University, Taichung 40704, Taiwan
[2]College of Mechanical and Electrical Engineering, Wenzhou University, Wenzhou 325035, China

Corresponding author: Jiawei Xiang (jwxiang@wzu.edu.cn)

This work was supported in part by the Zhejiang Special Support Program for High-level Personnel Recruitment of China under Grant 2018R52034, and in part by the Key Technologies Research and Development Program of Wenzhou of China under Grant 2018ZG023.

ABSTRACT This paper presents an optimization scheme to better design phononic crystals. A locally resonant phononic crystal (LRPC) structure called square spiral with circle inside is employed to verify the performance of the present scheme. Four geometric parameters, i.e., the side length of square scatterer, the length of each elastic beam, the thickness of elastic beams, and the radii of inner circles, are considered to obtain the corresponding influences on band gaps (BGs) using finite element method (FEM). According to the significant influences of the late two key parameters, a 2-factor (the radii of inner circles, and the thickness of elastic beams) and 7-level experiment is designed to obtain optimal BGs with better low-frequency broadband properties. By 29 times calculations using FEM for the different combination of levels, three relationships between the 2-factor and the first BG's starting frequency, the first BG's bandwidth, and the second BG's bandwidth, are obtained and severed as inputs to the software of response surface methodology (RSM). The closed-form expressions of the three relationships are finally obtained to construct optimization models and result in the optimal band gaps (BGs) between 190-300*Hz* and 500-600*Hz*. It is expected that the present optimization scheme can be extended to material design of phononic/photonic structures in a reasonable way.

INDEX TERMS Locally resonant phononic crystals, response surface methodology, FEM simulations, band gaps, optimization.

I. INTRODUCTION

The noise and vibration in human life disturb the residents and even do harmful to the mental of them [1]–[5]. The frequencies of noise in human life are typically in the range of 100-1000 *Hz*. Earlier, some techniques of noise cancellation and vibration suppression were proposed, i.e. the design and selection of structural modal parameters [6], utilizing dynamic absorber [7], vibration isolation mass [8], active noise control [9], active vibration control [10] and active structural acoustic control [11], etc. Recently, as a newly noise cancellation and vibration suppression concept, phononic crystals (PCs) [12] has achieved significant progress, and a lot of new phononic crystal structures were proposed and attempted to be used for the noise cancellation and vibration suppression [13]–[17].

The associate editor coordinating the review of this manuscript and approving it for publication was Jiansong Liu.

However, in the early stage of the phonoic crystal development, PCs were commonly computed with the Bragg scattering mechanism. The corresponding BGs reached over hundred thousand *Hz*, which were unsuitable for the demand of lower frequency and wider band gaps (BGs) [18]. In order to overcome this problem, Liu et al. proposed a locally resonant phononic crystal (LRPC) with much lower BGs [18]. Consequently, numerous two-dimensional (2D) and three-dimensional (3D) LRPCs structures were designed to be possibly applied to many scenarios of the noise cancellation and vibration suppression [19]–[25]. Meanwhile, numerical simulation methods were developed to help the analysis and design of LRPCs structures, such as finite element method (FEM) [26]–[28], boundary element method (BEM) [29], wavelet-based FEM [30], lumped-parameter model [31], singularity expansion method [32], [33] etc. It point out that photonic crystals [34] have been succeed applied to many engineering application area. However, to meet the real-world applications, the search for specific LRPC structures is still in progress. Moreover, Wu and his team did systematically theoretical and experimental investigations about LRPCs structures, which show that the numerical simulations are in a certain agreement with experimental rusts [27], [32], [33]. Therefore, the numerical simulation, especially FEM can be employed as a useful tool to design LRPCs structures. However, few literatures focus on the optimization scheme of LRPCs structures.

On the foundation of the structure data obtained by a sequence of designed experiments, the response surface methodology (RSM) is an analysis approach which can explore the functions relevance between several factor variables and one or more response variables in calculating the structure data [35]. Song et al. proposed a mechanical parameters detection method using the FEM and RSM [36], [37].

Motivated by the FEM simulation-based optimization method, we develop a structural parameters optimization scheme to obtain relatively optimal LRPC structures by combination of the FEM simulations and RSM analysis. More specifically, a spiral LRPC structure is designed has low-frequency and wide band properties. Firstly, the LRPC of square spiral with circle inside is given and the corresponding band structures are calculated by FEM. Three key geometric parameters are analyzed and only the two parameters are significant. Secondly, a 2-factor and 7-level experiment is devised to perform the RSM analysis to obtain the closed-form expressions of the three relationships between structural parameters and BGs. Finally, the data are referenced after computed, and the functional combinations are obtained between the BGs and the geometric parameters. Finally, by solve the constructed optimization models, the optimal band gaps (BGs) are obtained using interior point method (IPT). It notes that the band structures analyzed in this research are supposed to the only propagating modes.

II. THE STRUCTURE OF A UNIT CELL

A. A SQUARE SPIRAL WITH CIRCLE INSIDE

Fig.1. shows two unit cells for the LRPC of square spiral with four circles inside, which is nominated as M_1 and M_2, respectively. Obviously, each LRPC structure has four spiral elastic beams surround the four circle/arc elastic beams, and the scatterer is embedding in the center of the structure. The spirals are on each side of the LRPC have two horizontal and three vertical elastic beams. The unique difference between Figs.1(a) and (b) is the four circle and arc elastic beams.

As shown in Fig.1, a is the lattice constant of the unit cell, b is the unique thickness of elastic beams, c is the side length of square scatterer, r_1 is the radius of outer circle, r_2 is the radius of inner circle. Moreover, d, e, f, g, h, and i are the length of each elastic beam, respectively, and the thickness of the square frame is fixed to 5×10^{-4} m.

In the finite element simulations, the geometric parameters of M_1 are: $a = 32 \times 10^{-3}$ m, $b = 5 \times 10^{-4}$ m, $c = 8 \times 10^{-3}$ m, $d = 15 \times 10^{-3}$ m, $e = 5 \times 10^{-3}$ m, $f = 25.5 \times 10^{-3}$ m,

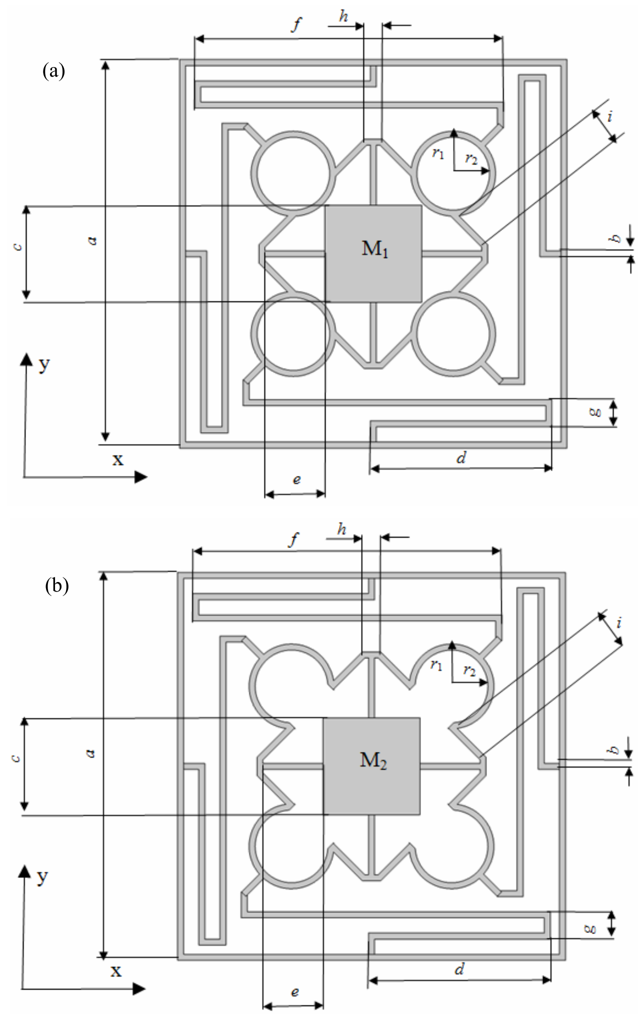

FIGURE 1. A unit cell named M_1 and M_2: (a) M_1, (b) M_2 (Unit: m).

TABLE 1. The mechanical parameters of the two materials.

Materials	Young's modulus $(E)Pa$	Density $(\rho)(Kg/m^3)$	Poisson's ratio(ν)
PA6	2.32×10^9	1180	0.34
Piezoelectric ceramic	76.5×10^9	7650	0.32

$g = 2.75 \times 10^{-3}$ m, $h = 1.53 \times 10^{-3}$ m, $i = 4 \times 10^{-3}$ m, $r_2 = 3 \times 10^{-3}$ m, $r_1 = 3.5 \times 10^{-3}$ m.

The material of elastic beams and the frame are PA6, and the scatterer is piezoelectric ceramic. The mechanical parameters of the two materials are listed in Table.1.

By utilizing FEM analysis software Comsol, the BGs are calculated. As shown in Fig.2, eight frequency bands are obtained and two BGs (the first BG: 201.5 Hz to 293.8 Hzin associate with P_1 and P_2, the second BG: 500.8 Hz to 607.3 Hzin associate with P_3 and P_4) are clearly shown between the dash line Q_1 and $Q_{2,}$, Q_3 and Q_4, respectively, where Q_1 and Q_2 denote the lower and upper edges (the starting and

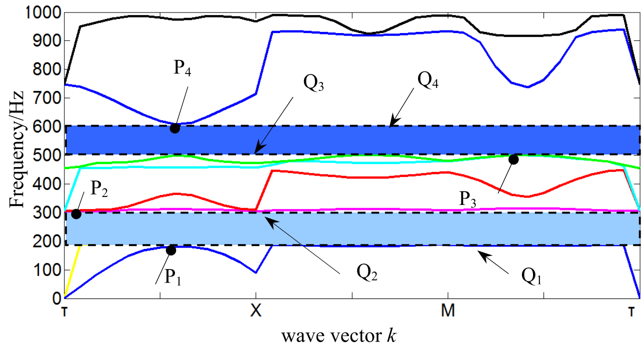

FIGURE 2. The band structures of M_1 (piezoelectric ceramic).

terminal frequencies) of the first BG, Q_3 and Q_4 represent the lower and upper edges (the starting and terminal frequencies) of the second BG. It notes that the wave vector k of P_1, P_2, P_3, and P_4 are: 0.5833, 0.0833, 2.4167 and 0.5833.

The displacement mode shape of M_1 in associate with Q_1, $Q_{2,}$, Q_3 and Q_4 are shown in Fig.3.

From Fig.3, the vibration of P_1 is concentrated in upper-lower beams. The deformations of the upper-lower beams are large, whereas the frame remains unchanged. Moreover, the deformations of the scatterer and the right-left beams are small. For displacement mode shape of P_2, vibration is centralized in the right-left beams, the magnitude of deformation is small in the upper-lower beams and the frame, and the scatterer is little affected by the vibration. For P_3, the deformations are similar to P_1. In mode shape P_4, the four beams are out of shape, and the frame and scatterer are presenting torsional mode.

In Table.1, the Young's modulus and density of elastic beams and the frame are much lower than those of the scatterer. Therefore, the vibration pattern is exactly a mass-spring system, the scatterer can represent the mass and the elastic beams act as the mechanical springs. Under the procedure of the Mie scattering, the low-frequency longitudinal wave is converted into the transverse wave. The scatterer transverse has a greater impact in every unit cell, because of the destructive interference, and then the two main BGs are engendered around the center mass (the scatterer) resonant frequencies.

Generally, LRPC BGs are dependent on the mass of scatterer. If we use a material with a higher density (lead) than ceramic as the scatterer material, the band structures are shown in Fig.4. The first BG: 156.4 Hz to 285.2 Hzin associate with U_1 and U_2, the second BG: 456.5 Hz to 567.6 Hzin associate with U_3 and U_4. Compared with Fig.2, it obviously the starting frequencies of M_1(lead) is lower than those of M_1(piezoelectric ceramics) and the corresponding bandwidths are a little large.

However, in the present investigations, the higher density material of scatterer is not considered for we fixed the scatterer material to piezoelectric ceramics (might be used for energy harvest).

Moreover, the full four circles elastic beams of M_1 limits the range of motion of the scatterer. If we chose the four

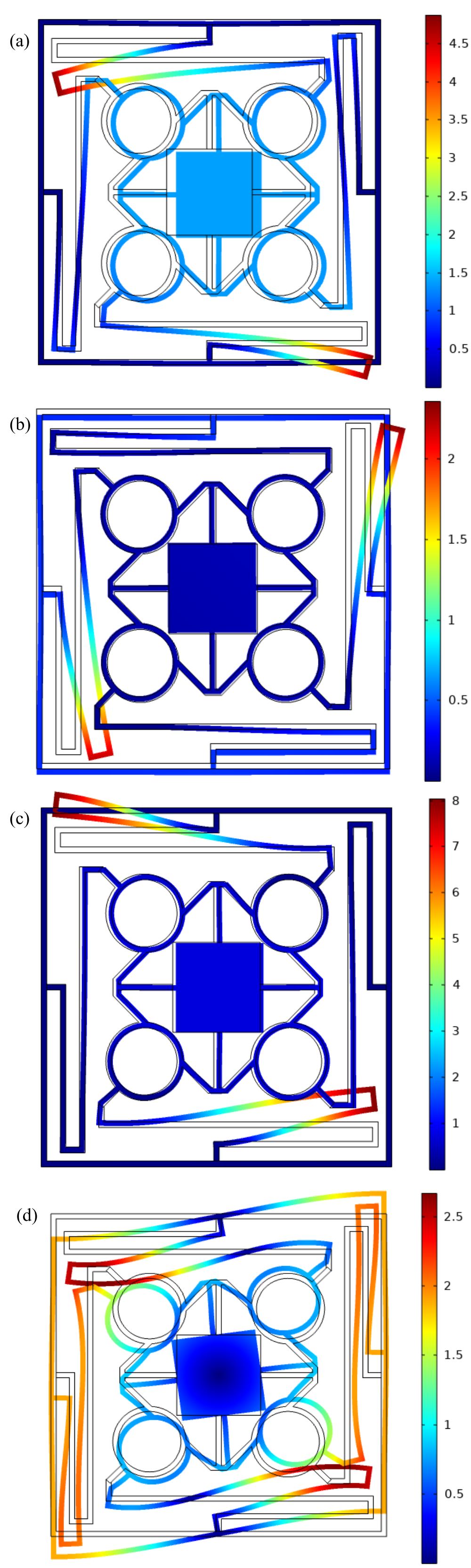

FIGURE 3. The displacement mode shape of M_1: (a) Q_1, (b) Q_2, (c) Q_3, (d) Q_4, corresponding to points P_1, P_2, P_3, and P_4, respectively.

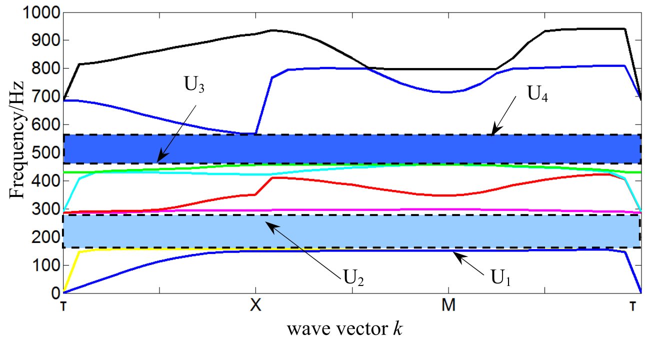

FIGURE 4. The band structures of M_1 (lead).

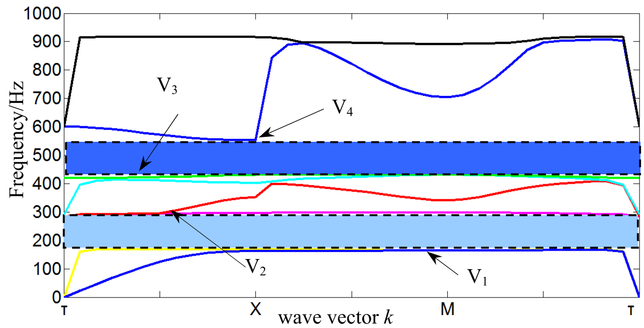

FIGURE 5. The band structures of M_2 (piezoelectric ceramics).

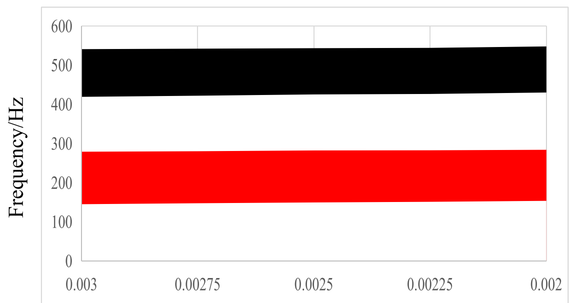

FIGURE 6. The influence of the length of the radii of inner arcs.

arc elastic beams of the LRPC structure (M_2), as shown in Fig.1(b), the band structures are shown in Fig.5. The first BG: 170.2 Hz to 284.3 Hzin associate with V_1 and V_2, the second BG: 432.7 Hz to 553.4 Hzin associate with V_3 and V_4. Compared with Fig.2, the starting frequencies of M_2(piezoelectric ceramics) is lower than those of M_1(piezoelectric ceramics), and the two bandwidths are a little large.

However, as shown in Fig.6, the influence of BGs is monotonically increasing at the decreasing of radii of inner arcs. Therefore, it optimization scheme is unnecessary for such type of structures.

Generally, in the case of none optimization, the BGs of the LRPC is in the low frequency. However, the BGs are closely related to the resonant frequencies of the mass-spring system, which possibly influenced by geometric parameters. Therefore, it is possible to obtain optimal BGs by optimizing

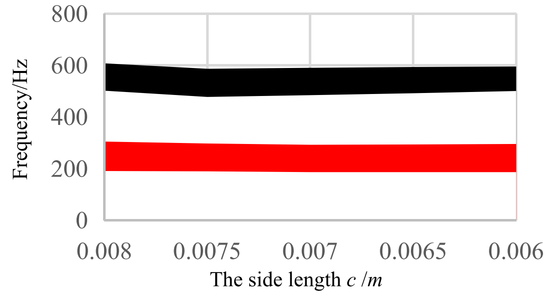

FIGURE 7. The influence of the side length.

the geometric parameters in the present LRPC of square spiral with four circles inside.

B. THE EFFECT OF THE SIDE LENGTH OF SQUARE SCATTER ON BGS

In this section, the impact of the side length of square scatterer c on the BGs is investigated. A series of the side length c (in the range of $6 \times 10^{-3}m$ to $8 \times 10^{-3}m$) are considered and the results are shown in Fig.7.

The upper and the lower edges of the red and black areas are the starting and terminal frequencies of the first and second BGs, respectively. The regularity of the red and black areas indicated that the variation of the starting and terminal frequencies is almost kept unique as c decreased. Therefore, the parameter c has very little effect on the BGs, which can be excluded from the key geometric parameters for BGs optimization.

C. THE EFFECT OF THE LENGTH OF EACH ELASTIC BEAM ON BGS

To investigate the influence of the length of each elastic beam, we take one of the length of elastic beam e (in the range of $5 \times 10^{-4}m$ to $17.5 \times 10^{-4}m$) for an example, the change of two BGs along with the length of elastic beam e, is shown in Fig.8 (a). We find that the variation of the bandwidth can be neglected (the upper and the lower edges of the two BGs are nearly smooth), therefore this parameter is also not the key parameter to influence BGs. Fig.8 (b) shows the change of two BGs along with the length of elastic beam d, both the two BGs are monotonously increasing or decreased and the original selection $d = 15 \times 10^{-3}$ m is the relatively best one. It notes that for the length of other elastic beams d, f, g, h, and i (shown in Fig.1), the influence laws are similar to e and d discussed herein.

D. THE EFFECT OF THE THICKNESS OF ELASTIC BEAMS ON BGS

The spiral turns are preclude owing to the limitation of the structure size. Therefore, we focus on the influence of the thickness of elastic beams b (from $5 \times 10^{-4}m$ to $15 \times 10^{-4}m$) and the results are shown in Fig.9. With the increase of b, the bandwidth of the first BG climbs up (from $5 \times 10^{-4}m$ to $7.5 \times 10^{-4}m$) and then declines (from 7.5×10^{-4} m to $15 \times 10^{-4}m$), whereas both the starting and terminal frequencies

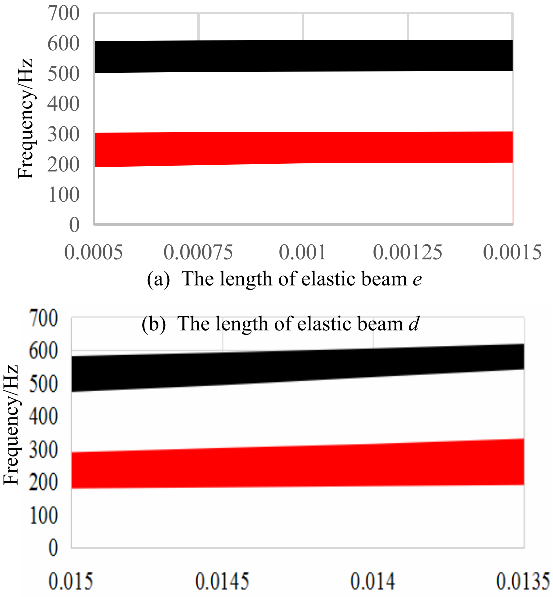

FIGURE 8. **The influence of the length of elastic beam e and d.**

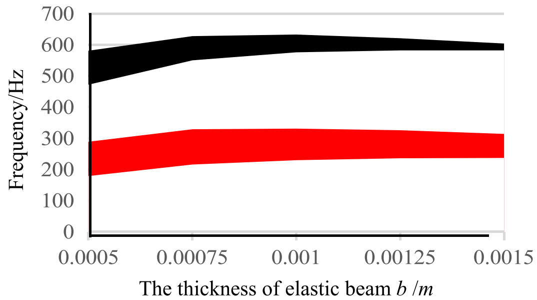

FIGURE 9. **The influence of the thickness of elastic beams.**

are increased. Moreover, as the b increase, the bandwidth of the second BG decrease, and the starting frequency of the second BG increase first and after that it preserves an approximate constant, the terminal frequency of second BG increases (from $5 \times 10^{-4}m$ to $10 \times 10^{-4}m$) and then dwindles (from $12.5 \times 10^{-4}m$ to $17.5 \times 10^{-4}m$), whereas the whole bandwidth decrease with a large b. From the above analysis, we find that the thickness b of elastic beams is a key parameter to obtain a relative optimization BGs.

E. THE EFFECT OF THE RADII OF INNER CIRCLES ON BGS

Generally, the obstructions of wave conduction of the ring beams are determined by the radii of inner circles. The four ring beams with the inner circle radii r_2 do effect on bandwidths of the BGs. Suppose r_2 is changed from $3 \times 10^{-3}m$ to $0m$, the results are given in Fig.10.

As illustrated in Fig.10, the unapparent trend of the starting and terminal frequencies of the first BG is manifest as slow decreasing, and the bandwidth is substantially retained. The main influence of the radii of inner circles is the second BG. The starting and terminal frequencies of the second BG is increases (r_2 is changed from $3 \times 10^{-3}m$ to $2.5 \times 10^{-3}m$)

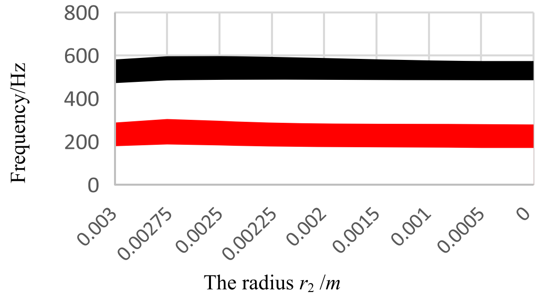

FIGURE 10. **The influence of the radii of inner circles.**

rapidly first and then decreases (r_2 is changed from $2.5 \times 10^{-3}m$ to $0m$) sluggishly. Moreover, the bandwidth of the second BG increases (r_2 is changed from $3 \times 10^{-3}m$ to $2.75 \times 10^{-3}m$) and then decreases (r_2 is changed from $2.75 \times 10^{-3}m$ to $0m$). In conclusion, the results indicate that r_2 do tiny contribute to the bandwidth of the first BG but the second BG is impacted greater.

Four geometric parameters, i.e., the side length of square scatterer c, the length of each elastic beam ed, f, g, h, and i, the thickness of elastic beams b, and the radii of inner circles r_2, are discussed to obtain the corresponding influences on BGs, and the significant influences of the late two key parameters b and r_2 are finally determined.

III. RSM ANALYSIS

RSM is a reasonable experimental design method to obtain data relationships for numerical and physical experiments. The functional relationship between factors and response values is fitted by multiple quadratic regression equation. In the present, the thickness of elastic beams b, and the radii of inner circles r_2 served as two factors; the first BG's starting frequency (indicate as I), the first BG's bandwidth (indicate as F), and the second BG's bandwidth (indicate as S) are severed response values. Therefore, the RSM can be employed to calculate the functional relationships between the factors and response values. To obtain more accurate functional relationships, 7-level of each factor is selected and hence a 2-factor and 7-level experiment is designed. The range of the two factors r_2 and b are restricted from $2 \times 10^{-3}m$ to $3 \times 10^{-3}m$ and $5 \times 10^{-4}m$ to $10 \times 10^{-4}m$, respectively. The RSM analysis is carried out by the software Design-expert involves the 29 combinations of r_2 and b under different level. By 29 times calculations using FEM analysis software Comsol, we obtain 29 values for I, F and S, respectively.

The third-order model is used for the RSM fitting of each response. Take the predicting I for example, the model fitting value (denoted by F-value) of the RSM is 1208.8, which has great significance and the corresponding "F-value" only reaches 0.01% error due to the uncertainty. Table.2 shows the characteristic value of the predicting I. The value of "R-Squared" is 0.9983 indicate that the coincidence degree between the experimental data and the predicting data is 99.83%. Moreover, the different between "Adj R-Squared" and "Pred R-Squared" is merely 0.08% means

TABLE 2. Characteristic value of the model.

Std. Dev.	2.05	R-Squared	0.9983
Mean	12.99	Adj R-Squared	0.9974
C.V. %	0.83	Pred R-Squared	0.9966
PRESS	155.21	Adeq Precision	104.09

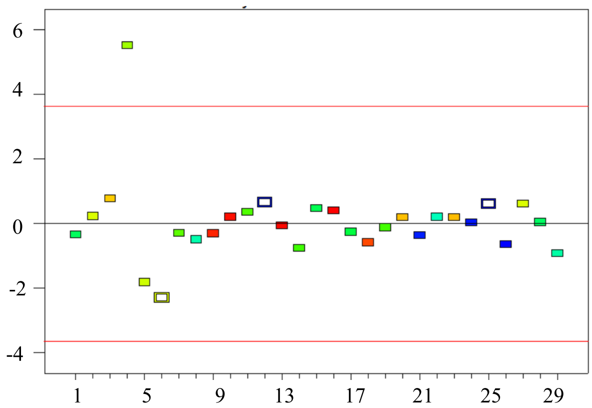

FIGURE 11. The externally studentized residuals.

that the regression result has remarkable effect. "Adeq Precision" attains 104.09, which is far outweigh the baseline value 4, and further proves the data is very adequate. More theoretical details about the RSM analysis can be seen in Ref. [35].

To further observe the residuals and to obtain the more accurately and more intuitive error exhibition, the graph of the externally studentized residuals is plotted in Fig.11. As shown in Fig.11, 96.6% points are in the range of -3 to 3, 93.1% points are in the range of -2 to 2, the distribution of those points are basically tallied with the properties of standard normal distribution.

Fig.12 shows the predicted versus actual 29 starting frequencies of the first BG using FEM analysis software Comsol. In Fig.12, we can see clear that every predicted value is almost entirely with the actual value. It represents that the accuracy of the functional relationship between the predicting I and the two key parameters r_2 and b is reliability.

The relationship between the 2-factor and the first BG's starting frequency for predicting I is obtained by RSM analysis and the closed-form expression is:

$$\begin{aligned} I = & 599.59642 - 80,81337 r_2 + 48.13497 b \\ & + 1.98902 r_2 b + 3.13163 r_2^2 - 4.59857 b^2 \\ & - 0.0325522 r_2^2 \text{b-}0.032385 r_2 b^2 \\ & - 0.040319 r_2^3 + 0.16102 \text{b}^3 \end{aligned} \tag{1}$$

At the same time, the closed-form expression of the relationship between the 2-factor and the first BG's bandwidth

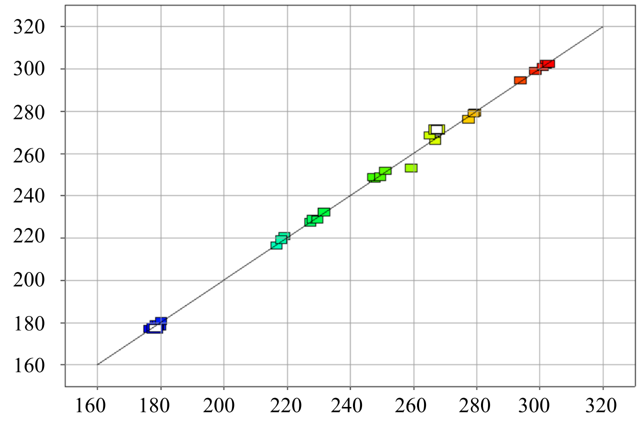

FIGURE 12. The Predicted v.s. Actual starting frequency (Hz) of the first BG.

for predicting F is represented by:

$$\begin{aligned} F = & -937.59512 + 48.72026 r_2 + 268.80315 b \\ & - 0.63195 r_2 b - 1.96564 r_2^2 - 32.30676 b^2 \\ & + 8.46116E - 003 r_2^2 b + 3.91916E - 003 r_2 b^2 \\ & + 0.026703 r_2^3 + 1.22532 b^3 \end{aligned} \tag{2}$$

And the predicting S for the second BG's bandwidth (the relationship between the 2-factor and the second BG's bandwidth) can be given by:

$$\begin{aligned} S = & 104.42560 - 59.21849 r_2 + 217.41900 b \\ & - 3.96664 r_2 b - 3.18057 r_2^2 - 26.95625 b^2 \\ & + 0.045822 r_2^2 b + 0.094892 r_2 b^2 \\ & - 0.048853 r_2^3 + 1.13884 b^3 \end{aligned} \tag{3}$$

The effect of the noise cancellation and vibration suppression in the present LRPC structure is impacted by the whole bandwidth. Therefore, the whole bandwidth is the total value of the predicting F and S, and the corresponding relationship can be expressed as $W = F + S$ based on equivalent weight method.

In view of these relationships, we can optimize the two key structural parameters r_2 and b.

IV. THE OPTIMIZATION AND VERIFICATION OF THE STRUCTURE

Based on the relationships calculated in the previous section, this section focuses on the optimization of the LRPC structure. To restrict the noise cancellation and vibration suppression frequency less than 200 Hz, we can construct a single-object optimization function based on $W = F + S$. Moreover, the range of I can be employed as a constrained condition for the objective function on the basis of the application situation below 200 Hz. Hence, I can be limited to equal or lower than 200 Hz. For the other two constrained conditions, r_2 and b can be restricted to $2 \times 10^{-3} m \leq r_2 \leq 3 \times 10^{-3} m$ and $5 \times 10^{-4} m \leq b \leq 10 \times 10^{-4} m$.

TABLE 3. The results of the final optimal BGs calculated using the interior point method.

b ($\times 10^{-4}m$)	r_2 ($\times 10^{-3}m$)	I (Hz)	F (Hz)	S (Hz)	W(Hz)
5.31	2.793	191.8	115.9	108.4	224.3

TABLE 4. The verification of the optimal BGs by FEM using the optimization geometric parameters of the LRPC structure.

b ($\times 10^{-4}m$)	r_2($\times 10^{-3}m$)	I(Hz)	F(Hz)	S(Hz)	W(Hz)
5.31	2.793	190.5	114.8	108.1	222.9

Based on the above analysis, the optimization model of the present LRPC structure is defined as:

$$\text{Maximum } W = F + S \tag{4}$$

$$s.t. \begin{cases} 2 \times 10^{-3}m \le r_2 \le 3 \times 10^{-3}m \\ 5 \times 10^{-4}m \le b \le 10 \times 10^{-4}m \\ I \le 200Hz \end{cases} \tag{5}$$

Interior point method is commonly used to deal with constrained optimization problems. After calculations, the results of the final optimal BGs are showed in Table.3.

Observing Table.3, the starting frequency of the first BG is obviously below 200 Hz, and the whole bandwidth is the widest comparing with the single-factor analysis in Section II. The ultimate aim is to obtain the optimal BGs, thus the optimal data are verified by FEM software Comsol using the optimal structural parameters $b = 5.31 \times 10^{-4}m$ and $r_2 = 2.793 \times 10^{-3}m$ (as shown in Table 3).

The verification results are shown in Table 4. Comparing with Table.3, b, r_2, I, F, S, and W are in good agree with those in Table 4. The absolute relative errors of I and W is 0.67% and 0.62%, respectively. According to the tiny errors, the present optimization scheme and the corresponding optimal LRPC structure can be extended to design material structures as well as to use for the noise cancellation and vibration suppression. It worthy to point out here that 29 combinations is the standard experimental design for 2-factor and 7-level experiment of the RSM analysis. The precision is also guaranteed by the readability analysis of RSM, as shown in Section III.

V. CONCLUSION

In this paper, an optimization scheme is proposed to better design phononic crystals. Take a LRPC structure for example, its BGs are calculated using FEM software Comsol. It is found that the present LPCR structure has the good BGs for for noise cancellation and vibration suppression in daily life. The influences of geometric parameters on BGs are investigated, which are including the side length of square scatterer c, the lengths of all elastic beams (e, d, f, g, h, and i), the thickness of elastic beams b, and the radii of inner circles r_2. Furthermore, the two key geometric parameters (b and r_2) on BGs are determined, and thereafter a 2-factor and 7-level experiment is designed to solve the optimal BGs using an optimization model solved by the interior point method. The optimal geometric parameters are: $r_2 = 2.793 \times 10^{-3}m$ and $b = 5.31 \times 10^{-4}m$, and the corresponding starting frequency of the first BG is 191.8Hz, the first BG's bandwidth $F = 115.9\ Hz$, the second BG's bandwidth $S = 108.4\ Hz$, and the whole bandwidth $W = 222.9\ Hz$.

It is notes that the presented LRPC structure can be applied in daily life to suppress frequency range from 200Hz-300Hz, 500-600Hz (e.g. the rumble of starting the car engine). In addition, this optimization scheme is generally can be used for other PCs to obtain the optimal BGs, or can be employed to help the new material design with better properties.

Except for the noise cancellation and vibration suppression usage of the present optimization scheme, the LRPC of square spiral with circle inside or other LRPC structures can also be extended to support signal acquisition to filter out low frequency components (rotary speed and its harmonics) and retain high frequency components (fault features) for fault detection in mechanical systems [38]–[40] when the accelerometers are mounted on the LRPC plate. It is worthy of point out that the relatively complex LRPC structures are still in trial running. Therefore, the further work is to produce physical LRPC structures (composite structures) using a 3D printer (might be technological maturity soon) and tested in the anechoic chamber to prove the good performance.

REFERENCES

[1] A. H. Aly and A. Mehaney, "Phononic crystals with one-dimensional defect as sensor materials," *Indian J. Phys.*, vol. 91, no. 9, pp. 1021–1028, Sep. 2017.

[2] H. Nassar, X. C. Xu, A. N. Norris, and G. L. Huang, "Modulated phononic crystals: Non-reciprocal wave propagation and Willis materials," *J. Mech. Phys. Solids.*, vol. 101, pp. 10–29, Jan. 2017.

[3] H. Gao, J. Xiang, C. Zheng, Y. Jiang, and T. Matsumoto, "BEM-based analysis of elastic banded material by using a contour integral method," *Eng. Anal. Boundary Elements*, vol. 53, pp. 56–64, Apr. 2015.

[4] M. Kurosu, D. Hatanaka, K. Onomitsu, and H. Yamaguchi, "On-chip temporal focusing of elastic waves in a phononic crystal waveguide," *Nat. Commun.*, vol. 9, p. 1331, Apr. 2018.

[5] M. Miniaci, A. S. Gliozzi, B. Morvan, A. Krushynska, F. Bosia, M. Scalerandi, and N. M. Pugno, "Proof of concept for an ultrasensitive technique to detect and localize sources of elastic nonlinearity using phononic crystals," *Phys. Rev. Lett.*, vol. 118, no. 21, May 2017, Art. no. 214301.

[6] C. F. Ng and C. K. Hui, "Low frequency sound insulation using stiffness control with honeycomb panels," *Appl. Acoust.*, vol. 69, no. 4, pp. 293–301, Apr. 2008.

[7] K. Idrisi, M. E. Johnson, A. Toso, and J. P. Carneal, "Increase in transmission loss of a double panel system by addition of mass inclusions to a poro-elastic layer: A comparison between theory and experiment," *J. Sound Vib.*, vol. 323, pp. 51–66, Jun. 2009.

[8] H. Wen, J. Guo, Y. Li, Y. Liu, and K. Zhang, "The transmissibility of a vibration isolation system with ball-screw inerter based on complex mass," *J. Low Freq. Noise, Vib. Act. Control*, vol. 37, no. 4, pp. 1097–1108, Dec. 2018.

[9] S. K. Lau and S. K. Tang, "Sound fields in a slightly damped rectangular enclosure under active control," *J. Sound Vib.*, vol. 238, no. 4, pp. 637–660, Dec. 2000.

[10] T. C. Sors and S. J. Elliott, "Volume velocity estimation with accelerometer arrays for active structural acoustic control," *J. Sound Vib.*, vol. 258, no. 5, pp. 867–883, Dec. 2002.

[11] J. P. Carneal and C. R. Fuller, "An analytical and experimental investigation of active structural acoustic control of noise transmission through double panel systems," *J. Sound Vib.*, vol. 272, nos. 3–5, pp. 749–771, May 2004.

[12] M. Kushwaha, P. Halevi, L. Dobrzynski, and B. Djafari-Rouhani, "Acoustic band structure of periodic elastic composites," *Phys. Rev. Lett.*, vol. 71, no. 13, pp. 2022–2025, Sep. 1993.

[13] X. Zhang and Z. Liu, "Negative refraction of acoustic waves in two-dimensional phononic crystals," *Appl. Phys. Lett.*, vol. 85, no. 2, pp. 341–343, Jul. 2004.

[14] Y.-F. Wang, Y.-S. Wang, and X.-X. Su, "Large bandgaps of two-dimensional phononic crystals with cross-like holes," *J. Appl. Phys.*, vol. 110, no. 11, Dec. 2011, Art. no. 113520.

[15] H. Dong, X.-X. Su, Y.-S. Wang, and C. Zhang, "Topological optimization of two-dimensional phononic crystals based on the finite element method and genetic algorithm," *Struct. Multidisciplinary Optim.*, vol. 50, no. 4, pp. 593–604, Oct. 2014.

[16] S. Jiang, H. Hu, and V. Laude, "Ultra-wide band gap in two-dimensional phononic crystal with combined convex and concave holes," *Phys. Status Solidi (RRL)-Rapid Res. Lett.*, vol. 12, no. 2, Feb. 2018, Art. no. 1700317.

[17] P. Li, G. Wang, D. Luo, and X. Cao, "Wave bandgap formation and its evolution in two-dimensional phononic crystals composed of rubber matrix with periodic steel quarter-cylinders," *Int. J. Mod. Phys. B*, vol. 32, no. 4, Feb. 2018, Art. no. 1850037.

[18] Z. Liu, X. Zhang, Y. Mao, Y. Y. Zhu, Z. Yang, C. T. Chan, and P. Sheng, "Locally resonant sonic materials," *Science*, vol. 289, pp. 1734–1736, Sep. 2000.

[19] H. Zhai, H. Xiang, X. Ma, and J. Xiang, "Optimization scheme of geometric parameters for a 2D locally resonant phononic crystal structure," *Jpn. J. Appl. Phys.*, vol. 58, no. 5, 2019, Art. no. 051001.

[20] M. Liu, J. Xiang, and Y. Zhong, "Band structures analysis method of two-dimensional phononic crystals using wavelet-based elements," *Crystals*, vol. 7, no. 11, p. 328, Oct. 2017.

[21] M. Liu, Y. Zhong, and J. Xiang, "The band gap and transmission characteristics investigation of local resonant quaternary phononic crystals with periodic coating," *Appl. Acoust.*, vol. 100, pp. 10–17, Dec. 2015.

[22] I. Psarobas, N. Stefanou, and A. Modinos, "Phononic crystals with planar defects," *Phys. Rev. B, Condens. Matter*, vol. 62, no. 9, pp. 5536–5540, Sep. 2000.

[23] J. Vasseur, P. A. Deymier, A. Khelif, P. Lambin, B. Djafari-Rouhani, A. Akjouj, L. Dobrzynski, N. Fettouhi, and J. Zemmouri, "Phononic crystal with low filling fraction and absolute acoustic band gap in the audible frequency range: A theoretical and experimental study," *Phys. Rev. E, Stat. Phys. Plasmas Fluids Relat. Interdiscip. Top.*, vol. 65, no. 5, May 2002, Art. no. 056608.

[24] W. Kuang, Z. Hou, and Y. Liu, "The effects of shapes and symmetries of scatterers on the phononic band gap in 2D phononic crystals," *Phys. Lett. A*, vol. 332, nos. 5–6, pp. 481–490, Nov. 2004.

[25] X. Zhang, Z. Liu, and Y. Liu, "The optimum elastic wave band gaps in three dimensional phononic crystals with local resonance," *Eur. Phys. J. B, Condens. Matter Complex Syst.*, vol. 42, no. 4, pp. 477–482, Dec. 2004.

[26] D. Yu, Y. Liu, G. Wang, L. Cai, and J. Qiu, "Low frequency torsional vibration gaps in the shaft with locally resonant structures," *Phys. Lett. A.*, vol. 348, nos. 3–6, pp. 410–415, Jan. 2006.

[27] S. W. Zhang, J. H. Wu, and Z. P. Hu, "Low-frequency locally resonant band-gaps in phononic crystal plates with periodic spiral resonators," *J. Appl. Phys.*, vol. 113, no. 16, Apr. 2014, Art. no. 163511.

[28] M. Oudich, M. B. Assouar, and Z. Hou, "Propagation of acoustic waves and waveguiding in a two-dimensional locally resonant phononic crystal plate," *Appl. Phy. Lett.*, vol. 97, no. 19, Nov. 2010, Art. no. 193503.

[29] H. Gao, T. Matsumoto, T. Takahashi, and H. Isakari, "Investigation of finite/infinite unidirectional elastic phononic plates by BEM," *Eng. Anal. Boundary Elements*, vol. 40, pp. 93–103, Mar. 2014.

[30] M. Liu, J. Xiang, H. Gao, Y. Jiang, Y. Zhou, and F. Li, "Research on band structure of one-dimensional phononic crystals based on wavelet finite element method," *Comput. Model. Eng. Sci.*, vol. 97, no. 5, pp. 425–436, Feb. 2014.

[31] K. Lu, J. W. Wu, L. Jing, and D. Guan, "Flexural vibration bandgaps in local resonance beam with a novel two-degree-of-freedom local resonance system," *Eur. Phys. J. Appl. Phys.*, vol. 77, no. 2, Feb. 2017, Art. no. 020501.

[32] P. Cao and J. H. Wu, "Shape recognition of acoustic scatterers using the singularity expansion method," *J. Appl. Phys.*, vol. 121, Feb. 2017, Art. no. 105103.

[33] P. Cao, J. H. Wu, X. Chen, and Z. Huang, "An approach to investigate the multiple-scattering problems based on the singularity expansion method," *J. Appl. Phys.*, vol. 123, Mar. 2018, Art. no. 135107.

[34] D. J. J. Hu, Z. Xu, and P. P. Shum, "Review on photonic crystal fibers with hybrid guiding mechanisms," *IEEE Access*, vol. 7, pp. 67469–67482, 2019.

[35] J. Cornell, *Experiments with Mixtures: Designs, Models, and the Analysis of Mixture Data*, 3rd ed. New York, NY, USA: Wiley, 2002, p. 123.

[36] W. Song, Y. Zhong, and J. Xiang, "Mechanical parameters detection in stepped shafts using the FEM based IET," *Smart Struct. Syst.*, vol. 20, no. 4, pp. 473–487, Oct. 2017.

[37] W. Song, J. Xiang, and Y. Zhong, "A simulation model based fault diagnosis method for bearings," *J. Intell. Fuzzy Syst.*, vol. 34, no. 6, pp. 3857–3867, Aug. 2018.

[38] S. Wang, J. Xiang, H. Tang, X. Liu, and Y. Zhong, "Minimum entropy deconvolution based on simulation-determined band pass filter to detect faults in axial piston pump bearings," *ISA Trans.*, vol. 88, pp. 186–198, May 2019.

[39] L. Wang and J. Xiang, "A two-stage method using spline-kernelled chirplet transform and angle synchronous averaging to detect faults at variable speed," *IEEE Access*, vol. 7, pp. 22471–22485, 2019.

[40] H. Liu and J. Xiang, "A strategy using variational mode decomposition, L-kurtosis and minimum entropy deconvolution to detect mechanical faults," *IEEE Access*, vol. 7, pp. 70564–70573, 2019.

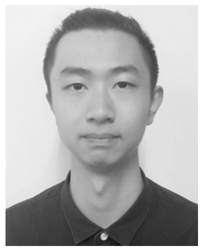

HANG XIANG is currently pursuing the bachelor's degree in applied physics with Tunghai University, Taiwan. His research interests include structural design and optimization of photonic and phononic crystals, and vibration measurement and analysis.

XINGFU MA received the B.S. degree in mechanical engineering from the Hubei University of Arts and Science, China, in 2018. He is currently pursuing the M.S. degree in mechanical engineering with Wenzhou University, China. His research interest includes photonic and phononic crystal materials and devices.

JIAWEI XIANG (M'19) received the B.S. degree in mechatronics from Hunan University, China, in 1997, the M.S. degree from Guangxi University, China, in 2003, and the Ph.D. degree from Xi'an Jiaotong University, China, in 2006. He is currently a Professor with the College of Mechanical and Electrical Engineering, Wenzhou University, China. His research interests include finite-element methods, phononic/photonics crystal materials and devices, health monitoring of mechanical systems using numerical simulation, signal processing, and artificial intelligence techniques.